Computational Materials Science 114 (2016) 199–208

Contents lists available at ScienceDirect

Computational Materials Science

journal homepage: www.elsevier.com/locate/commatsci

Hydrogen solubility in hcp titanium with the account of vacancy complexes and hydrides: A DFT study

D.O. Poletaev *, D.A. Aksyonov, Dat Duy Vo [1], A.G. Lipnitskii

The Center of Nanostructured Materials and Nanotechnologies, Belgorod State University, Belgorod, Russian Federation

ARTICLE INFO

Article history:
Received 24 August 2015
Received in revised form 14 December 2015
Accepted 21 December 2015
Available online 8 January 2016

Keywords:
Titanium
TiH hydrides
Hydrogen solubility
First-principles calculations

ABSTRACT

The saturation solubility of hydrogen with respect to titanium hydrides, and the concentration of H-vacancy complexes in α-Ti are predicted on the basis of a thermodynamic model and *ab initio* calculated free energies. The presence of hydrogen increases the vacancy complex concentration by several orders of magnitude, with most of these complexes containing three H atoms. We show also that the solubility of hydrogen within the titanium is strongly influenced by the temperature-dependent free energy terms, and that by including these terms in the thermodynamic model it is possible to obtain good agreement with experiment.

1. Introduction

For titanium alloys, hydrogen has significant importance from negative as well as positive points of view. On the one hand, the formation of hydrides causes embrittlement of all types of alloys such as $\alpha, \alpha+\beta$ and β alloys [1]. On the other hand, hydrogen is extensively used as a temporary alloying element providing the additional type of Ti alloys treatment known as thermohydrogen processing [2]. This treatment has several advantages; it increases tensile strength and ductility, improves sinterability of powder compacts, and leads to the grain refinement. Owing to the after-treatment removal of hydrogen, the further embrittlement is excluded.

Although, for binary Ti-H system, the influence of hydrogen has been extensively studied experimentally [3–10], still a lot of additional investigations are needed for more complex systems, which include the Ti alloys commonly used in industry (such as Ti–6Al–4V) and novel nanocrystalline Ti materials [11]. To improve the rate and quality of investigations, the experimental study should be complemented by computer simulation approaches, which provide unprecedented results on the atomic level and allow predicting multicomponent phase diagrams. However, there are many challenges on the way to a simulated phase diagram, which does not include experimental data. One of the examples of such challenges is the solubility limit of hydrogen. It was found that for beta alloys, such as Ti–Mo–Nb–Al [12] and Ti–V–Fe–Al [13], the embrittlement, due to hydrides formation, takes place at a concentration far below the solubility limit of 50 at.% in pure β-Ti. This shows that alloying elements could significantly influence the solubility of hydrogen, and its theoretical prediction would be useful.

However, the comparison of known experimental and theoretically calculated phase diagrams shows that the theory has failed to predict the solubility of hydrogen, even in pure α-Ti. For example, the experimental value of solubility at 600 K is of the order of 6.7 at.% [7], but in the work of Xu et al., based on first-principles and cluster expansion method, it is significantly underestimated (~1 at.%) [14]. Several factors could be responsible for this disagreement, but the most probable one is the omission of vibrational entropy and its influence on the hydrogen solution energy [14]. There are a number of studies, in which the Ti-H phase diagrams are assessed using thermodynamic approaches [15–18], however, in predicting the solubility, experimental data were used.

Coming back to the application of hydrogen as a temporary alloying element, we should mention that several positive effects caused by hydrogen, such as refinement of the structure after welding, improvement of powder alloys sintering, formation of a nanocrystalline structure, among others, are closely associated to the influence of hydrogen on diffusion processes [2]. Since the mechanisms of diffusion are determined by the vacancies in the material, the study of hydrogen-vacancy interaction is, therefore, very important. Indeed, the interaction of hydrogen with vacancies was extensively studied from first-principles [19], including the calculation of H diffusion coefficients [20,21]. However, despite

* Corresponding author. Tel.: +7 4722 58 54 08.
E-mail address: poletaev.dan@gmail.com (D.O. Poletaev).
[1] Present address: Institute for Computational Science (INCOS), Ton Duc Thang University, Viet Nam.

http://dx.doi.org/10.1016/j.commatsci.2015.12.037
0927-0256/

the experimental indications, the influence of hydrogen on the vacancy concentration was never evaluated [22].

Keeping in mind the problems outlined above, the aim of our work is to estimate the impact of vibrational entropy on the solubility of hydrogen, and to predict H influence on the vacancy concentration in α-Ti. In order to calculate the free energies of constituents at zero and finite temperatures, we use first-principles density functional theory in combination with harmonic approximation. In assessing the Ti-H hydrides, we extensively study the influence of c/a ratio on their formation energies and stability. Finally, the investigation of hydrogen influence on vacancy concentration is carried out with the help of a recently developed model for superabundant vacancy (SAV) description [23].

2. Computational details

To optimize the geometry of considered Ti-H structures and calculate their total energies we used ABINIT [24] and VASP [25] *ab initio* packages. Both packages implement density functional theory (DFT) [26,27] using plane-wave basis set and support projected augmented wave (PAW) formalism [28].

To describe $3s, 3p, 4s, 3d$ valence electrons of titanium (12 electrons in total) and $1s$ electron of hydrogen we have used PAW potentials constructed within the generalized gradient approximation (GGA) of the Perdew-Burke-Ernzerhof (PBE) form [29]. To ensure the convergence of results the following calculation parameters were chosen. The kinetic energy cutoff was set to 700 and 441 eV for ABINIT and VASP calculations, respectively. The spacing between k-points in the Brillouin-zone was ~ 0.15 Å^{-1}. The smearing of the Fermi surface was obtained with the Methfessel-Paxton method [30] and a smearing width of 0.14 eV and 0.2 eV was used in ABINIT and VASP calculations. Finally, the full structural relaxations were performed until the forces acting on atoms were less than 2.5 meV/Å in ABINIT calculations and 5 meV/Å in VASP calculations.

To insure that VASP and ABINIT packages provide consistent results, a number of calculations were performed twice. It was found that the results obtained with different packages are very close to each other. From the results obtained with ABINIT, we present the formation energies of 27 titanium hydrides depending on c/a ratio, thermal properties for three hydrides, and the formation energies of H-vacancy complexes. All other presented results, including thermal properties and formation energy of δ-TiH_2 relative to H solid solution, were obtained with VASP code.

To calculate cohesive energy of H_2 molecule in vacuum we have used $10 \times 10 \times 10$ Å supercell, which ensured convergence in total energy of 0.1 meV per one H atom. The titanium hydrides with different stoichiometry were constructed using face centered cubic (fcc) Ti supercell with four titanium atoms (cubic supercell). To model the hydrogen solid solution the $3 \times 3 \times 3$ ($Ti_{54}H$) hcp-Ti supercell was found to be enough to reproduce the solution energy with 8 meV precision.

To find stable positions of the H atoms inside the titanium vacancy three stages of relaxation were applied in the following order: (i) molecular dynamics simulation at 300 K with the velocity Verlet algorithm [31]; (ii) cooling down to 100 K using Nose–Hoover thermostat [32]; (iii) relaxation of the obtained supercells using Broyden-Fletcher-Goldfarb-Schano method [33] at 0 K.

To account the contribution of lattice vibrations in the free energies, we calculated them using harmonic approximation. The phonon densities of states (PHDOS) were calculated on the $36 \times 36 \times 36$ q-point grid through the diagonalization of the dynamical matrix at each q-point as implemented in the PHONOPY code [34].

The force constants required for construction of the dynamical matrix were computed using direct supercell approach. In this approach, the non-equivalent atoms are displaced in most symmetrical directions after which the resulting Hellmann–Feynman forces acting on atoms are calculated. The displacement step was 0.03 Å. For hydrides and hcp solid solution the force constants were calculated in $2 \times 2 \times 2$ cubic fcc-Ti supercell with 32 Ti atoms and $3 \times 3 \times 3$ hcp-Ti supercell with 54 Ti atoms, respectively.

3. Structure and energy of constituents in Ti-H system at 0 K

To determine the solubility of hydrogen, one has to first consider the constituents involved in the system and determine their free energies. In the current work, in order to reduce the complexity of the considered system, we omit the titanium bcc phase (β-Ti) from the evaluation. For this reason, our model Ti-H system includes gaseous H_2, hydrogen solid solution in hcp titanium (α-Ti), several titanium hydrides (TiH_x), and H-vacancy complexes. Since we completely rely on first-principles data, and do not use empirical fitting to the experiment (except the free energy of H_2 gas taken from NIST-JANAF tables [35]), it is natural to first describe all constituents at zero Kelvin temperature.

3.1. The description of gaseous H_2 phase and H solid solution in α-Ti

The free energy of H_2 gas is shifted by a certain value depending on the chosen PAW potentials. At zero pressure and zero temperature, we define the chemical potential of hydrogen as half of the energy of a H_2 molecule in vacuum, which is –3.383 eV for H potential used in VASP. The calculated values of the cohesive energy E_c and bond length of H_2 molecule are 4.544 eV and 0.751 Å, respectively. They are in good agreement with experimental values of 4.748 eV and 0.742 Å [10], and theoretical values of 4.532 eV and 0.746 Å obtained by Tao et al. using the PAW GGA approach [36].

For pure α-Ti, we obtained the lattice parameters $a = 2.937$ Å and $c = 4.646$ Å, which are in good agreement with experimental as well as previously calculated results [37,38]. To model the hydrogen solid solution, we put H into octahedral and tetrahedral interstitial voids of α-Ti. According to the recent studies, the H solution energies in these types of voids are very close (–0.62 eV and –0.56 eV at 0 K [20]), meaning that accounting of both interstitial types is needed for correct predictions of H solubility.

It is assumed that the approximation of dilute solid solution could be applied to the hydrogen in α-Ti [14]. This could be appropriate for the concentrations lower than 1 at.%, however it is known that the maximum solubility of H in α-Ti reaches ~6.7 at.% and for such concentration the distances between H atoms are of the order of 6 Å, at which noticeable interactions could exist. To check this, we considered several hcp-Ti supercells which model different concentration regimes: Ti_2H ($1 \times 1 \times 1$), Ti_8H ($2 \times 2 \times 1$), $Ti_{16}H$ ($2 \times 2 \times 2$), $Ti_{54}H$ ($3 \times 3 \times 3$), and $Ti_{96}H$ ($4 \times 4 \times 3$).

The solution energies and volumes of hydrogen in α-Ti per one H atom at 0 K were calculated as follows:

$$\begin{aligned} \Delta E_{sol} &= E(\mathrm{Ti}_m\mathrm{H}) - E(\mathrm{Ti}_m) - \frac{1}{2}E(\mathrm{H}_2), \\ \Delta V_{sol} &= V(\mathrm{Ti}_m\mathrm{H}) - V(\mathrm{Ti}_m), \end{aligned} \quad (1)$$

where $E(\mathrm{Ti}_m\mathrm{H})$ and $V(\mathrm{Ti}_m\mathrm{H})$ are the total energy and volume of supercell containing m Ti atoms and one H atom in octahedral or tetrahedral void, $E(\mathrm{Ti}_m)$ and $V(\mathrm{Ti}_m)$ are the total energy and volume of corresponding supercell with pure α-Ti, and $E(\mathrm{H}_2)$ is the total energy of hydrogen molecule in vacuum. The values of solution

Table 1
Energies (eV/atom-H) and volumes (Å^3) of hydrogen solution in octahedral and tetrahedral sites of hcp titanium along with c/a ratio depending on the size of the supercell.

Cell	ΔE_{sol},	c/a	ΔV_{sol}
Ti_2H	−0.461	1.606	1.49
Ti_8H	−0.441	1.586	1.68
$Ti_{16}H$	−0.457	1.583	1.76
$Ti_{16}H$ [39]	−0.471	–	–
$Ti_{54}H$	−0.417	1.582	1.71
$Ti_{54}H$ [39]	−0.426	–	1.78
$Ti_{96}H$	−0.425	1.583	1.82
$Ti_{54}H$(tetrahedral)	−0.353	1.583	3.51

energies and volumetric changes per one H atom are collected in Table 1.

It could be seen from Table 1 that the solution energy of hydrogen calculated from $Ti_{54}H$ supercell has converged to 8 meV and could be used for hydrogen solution description in the dilute regime. The value of solution energy obtained from $Ti_{16}H$ supercell (~5.9 at.%) is lower by 40 meV, which points out the existence of attractive interaction between hydrogen atoms with the increase of concentration. Since the magnitude of the interaction is quite small, we neglect it in the current study, and for solubility predictions, we use the solution energy obtained from $Ti_{54}H$ supercell.

According to our results, the solution energy of hydrogen in a tetrahedral site is higher than that in octahedral site by 64 meV. This is in agreement with the value of 60 meV obtained by Kuksin et al. using PAW GGA calculations [20].

The solution volumes of hydrogen are slightly higher for larger supercells (see Table 1). The values of volumes obtained from $Ti_{54}H$ cell are quite reasonable. They are 1.7 and 3.5 Å^3 for H in octahedral and tetrahedral sites, respectively, and are in good agreement with experimentally obtained average value of 3 Å^3 in fcc metals [40].

Finally, it is clear from Table 1 that c/a ratio in small cells is higher than that in pure Ti, meaning that hydrogen expands the hcp lattice in c direction.

3.2. The description of Ti-H phases

To model the titanium hydrides, we consider them as ordered structures with different H/Ti ratios and atomic configurations. The common formula unit for titanium hydrides is TiH_x, and their structure is based on the face centered cubic or face centered tetragonal (fct) titanium sublattice where hydrogen atoms are located in tetrahedral interstices. As found earlier in experimental [41] and theoretical works [14,36,42], the lattice constants and the level of tetragonal distortion (deviation of the lattice constants ratio (c/a) from unity) of the fcc lattice depend on the concentration of hydrogen in titanium hydride. In the literature regarding previous studies on the subject, three types of titanium hydrides depending on their structure are found: high temperature δ hydride with $c/a = 1$ and random occupation of interstices by H, low temperature ordered ϵ hydride with $c/a < 1$, and ordered γ hydride with $c/a > 1$.

The δ-titanium hydride with cubic symmetry is a non-stoichiometric phase, which, according to the Ti-H phase diagrams [43,17,18,44], is stable within the composition range from $TiH_{1.5}$ to TiH_2. At high hydrogen content and temperatures lower than 310 K there is a tetragonal transformation of the δ hydride into the ϵ hydride accompanied by the formation of ordered TiH_2 structure [41,45–47].

The precipitation of γ hydrides from the H solid solution in α-Ti matrix was experimentally observed several times, especially for low H concentrations [5,9,48–53]. It was found that γ hydrides have TiH stoichiometry, and the c/a ratio of their crystal cells varies from 1.08 to 1.12. Numakura and Koiwa [5] assumed that the structure of γ-TiH hydride matches with that of γ-ZrH, where hydrogen atoms occupy only half of the tetrahedral interstices, located in the {110} crystallographic planes. The latter theoretical works confirmed this assumption [14,36,42]. For a long time, the stability of γ hydride was debated. However, according to the recent first-principles investigations [14], the γ hydride is found to be thermodynamically metastable. The experimental observation of γ hydride is then explained by its coherent precipitation in α-Ti and the accompanied stabilization due to the internal tensile stresses.

While it is relatively easy to consider ordered stoichiometric phases such as ϵ-TiH_2 and γ-TiH from first-principles, the correct description of non-stoichiometric δ-TiH_x requires many more calculations. In order to take into account all possible tetragonal transformations, we found equilibrium lattice parameters and c/a ratio for 27 hydrides with symmetrically non-equivalent atomic configurations at different H/Ti ratios. In order to obtain hydrides with different stoichiometry, we used supercell with 4 Ti atoms and 1 to 8 H atoms. The structure of supercell is shown in Fig. 1, where possible positions of H atoms are designated by letters from "a" to "h".

To find optimized values of c/a ratio, we used the scheme proposed by Liang et al. [42]. According to this scheme, we changed the c/a ratio from 0.8 to 1.2 with an incremental step of 0.01 followed by volume and ionic optimization. With this approach, we found all local energy minima for configurations, which are symmetrically equivalent at $c/a = 1$, but become inequivalent under tetragonal distortion of the fcc lattice. For each configuration, the specific formation energies were calculated as follows:

$$\Delta E_f = \frac{E(Ti_4H_{4x}) - 4E(Ti_{hcp}) - 2xE(H_2)}{4x}, \quad (2)$$

where $E(Ti_4H_{4x})$ is the total energy of hydride supercell with 4 titanium atoms and $4x$ hydrogen atoms (x is the H/Ti ratio), $E(Ti_{hcp})$ is the total energy of titanium atom in hcp structure and $E(H_2)$ is the total energy of hydrogen atom in H_2 molecule.

The formation energies of all considered hydrides depending upon c/a ratio are shown in Fig. 2. According to Fig. 2, the following features are seen. The $TiH_{0.25}$, $TiH_{0.5}$, $TiH_{0.75}$, TiH, and $TiH_{1.25}$ hydrides have only one energy minimum in the whole range of c/a ratios. Finally, $TiH_{1.5}$(abcfgh), $TiH_{1.75}$, and TiH_2 hydrides have two energy minima, which are situated at $c/a < 1$ and $c/a > 1$. For all three phases, the first minimum at $c/a < 1$ is slightly lower by energy (<5 meV) than the second minimum. The existence of two minima and the favorability of tetragonal variant with $c/a < 1$ are in agreement with experimental findings [45] and other theoretical predictions [14,36,42,54]. It should be noted that in agreement with [36] only for $TiH_{0.25}$ hydride, the configuration with hydrogen atom in octahedral site is more favorable than that with hydrogen in tetrahedral site.

To compare formation energies of Ti-H phases with those in other theoretical works [36,42], we recalculated them per one Ti atom for configurations with the lowest energies:

$$\Delta H_f = x * \Delta E_f.$$

The results of comparison are collected in Table 2 and are shown in Fig. 3.

It is obvious from Fig. 3 that the slope of our curve is very close to that obtained by Liang et al. [42] and Tao et al. [36]. However, the values of formation energies are shifted by 5–17 kJ/mol-Ti. This shift could be associated to the chosen PAW potentials and the used number of valence electrons for Ti atom. In the current paper, we considered 12 valence electrons for titanium atom. At the same

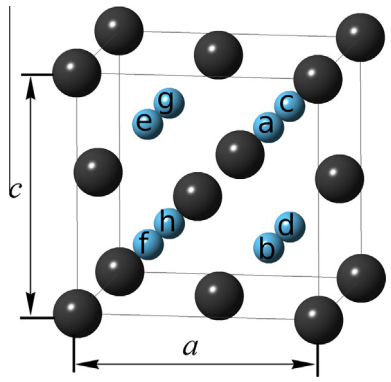

Fig. 1. The atomic structure of supercell used for different titanium hydrides. The possible positions for hydrogen atoms are designated by letters from "a" to "h".

time, the comparison of Ti-H lattice constants with that obtained in other works shows rather good agreement (see Table 2).

3.3. The stability of γ-TiH hydride

The γ-TiH hydride deserves special attention. Xu et al. [14], using first-principles calculations, obtained that γ-TiH hydride is unstable in relation to α-Ti and δ-TiH_2 at 0 K. In other words, the authors obtained that formation of γ-TiH is unfavorable according to the following reaction: δ-TiH_2 + α-Ti → 2(γ-TiH). The energy change ΔE, in this reaction, could be determined from the formation enthalpies ΔH_f of δ-TiH_2 and γ-TiH hydrides as

$$\Delta E = 2\Delta H_f(\mathrm{TiH}) - \Delta H_f(\mathrm{TiH_2}). \quad (3)$$

The value of ΔE could not be obtained from the data provided by Xu et al. but since the γ-TiH is unstable, the ΔE should be positive. However, we found that in our calculations, the ΔE is negative and equal to −15 meV. Our result is also in qualitative agreement with the works of Liang et al. [42] and Tao et al. [36], in which the values of ΔE are equal to −35 meV and −58 meV, respectively. It is quite difficult to explain the discrepancy in the literature data, since the authors used VASP code, PAW GGA potentials, and similar convergence parameters in all three cited papers. We expect that our result is more reliable due to the larger cut-off energy and PAW potential with 12 valence electrons.

3.4. Formation energies of hydrogen-vacancy complexes in hcp titanium

According to DFT calculations, titanium vacancy in α-Ti could trap up to three hydrogen atoms with the reduction of total energy [19]. From the thermodynamic point of view, the process of hydrogen trapping is equivalent to the reduction of effective vacancy formation energy, and it leads to the increase of vacancy concentration [23]. To determine the effect of hydrogen on vacancy concentration, it is important to know the formation energies of H-vacancy complexes. The formation process of H-vacancy complex consists of: (i) formation of Ti monovacancy; (ii) trapping of n hydrogen atoms from octahedral sites of the hcp-Ti lattice.

In our study, the formation energy of H-vacancy complex with n H atoms (n = 0–5) is calculated as

$$E_f^{vac,n} = E(\mathrm{Ti_{35}H_n^{vac}}) - \frac{35}{36}E(\mathrm{Ti_{36}}) - n[E(\mathrm{Ti_{36}H}) - E(\mathrm{Ti_{36}})], \quad (4)$$

where $E(\mathrm{Ti_{35}H_n^{vac}})$, $E(\mathrm{Ti_{36}H})$ and $E(\mathrm{Ti_{36}})$ are the total energies of commensurate hcp Ti supercells with vacancy and n H atoms, with one H atom in octahedral site, and without any defects, respectively. The calculated values of $E_f^{vac,n}$ in comparison to literature results are collected in Table 3.

The trapping energy associated to the addition of each subsequent H atom into the H-vacancy complex with n H atoms is defined as

$$\Delta E^{trap} = E_f^{vac,n+1} - E_f^{vac,n} \quad (5)$$

and is also provided in Table 3. If the value of ΔE^{trap} is negative, then the transition of a hydrogen atom from octahedral site to the H-vacancy complex is energetically favorable process. According to our results, the titanium vacancy could trap up to four H atoms, which is more than what was found by Connetable et al. [19]. In agreement with [19], the addition of the fifth atom is unfavorable.

It should be noted that there is a small almost constant difference (∼160 meV) between our vacancy formation energies and the energies obtained in [19] (see Table 3). This is related to the usage of larger supercell by Connetable et al. [19] (with 95 Ti atoms), which means that their results are technically more reliable. Nevertheless, the values of trapping energies are almost the same.

Since we have found additional favorable H-vacancy complex with four H atoms and for the sake of consistency, we continue to use our result in further estimations of vacancy concentrations. It is known that GGA approximation poorly treats vacancies, and their formation energies obtained for larger supercell are still biased from the experimental values. Hence, only the qualitative estimations of hydrogen influence on vacancy concentration make sense.

4. Thermodynamic properties of constituents at finite temperatures

The formation energies of Ti-H phases and H solid solution obtained at 0 K, in first approximation, could be used for the calculation of the H solubility in α-Ti. However, to increase the quality of predictions, as a second step, one should take into account the temperature dependence of vibrational energy and entropy of atoms in the considered constituents. The corrections related to the zero-point vibrational contributions are especially important for the H containing systems due to the low hydrogen mass.

To calculate the vibrational free energy of compound at finite temperatures, we use harmonic approximation, which is appropriate to provide good agreement with experimental data for Ti-H system [59]. It was found that phonons determine the temperature dependencies of Ti-H thermodynamic properties in much higher degree than electrons [42,59]. For example, the electron contribution to the isochoric heat capacity of TiH_2 [42] does not exceed the value of 5 J/mol/K, which is less than 7% of the phonon contribution to the heat capacity even at temperatures >1000 K. Hence, in our consideration, we neglected the influence of electron free energy on solubility.

4.1. Free energy of hydrogen solid solution in α-Ti

For assessing H solid solution at finite temperatures, we used an approximation of dilute solution and considered only hydrogen in octahedral interstitial sites of hcp lattice. To compare our results with the experiment, we calculated the solution enthalpy of hydrogen in the hcp lattice of titanium at zero pressure as

$$\Delta H_{sol}(T) = \Delta E_{sol} + E_{vib}^{\mathrm{Ti_{54}H}}(T) - E_{vib}^{\mathrm{Ti_{54}}}(T) - \frac{1}{2}E^{\mathrm{H_2}}(T), \quad (6)$$

where ΔE_{sol} is the solution energy at 0 K defined by the Eq. (1), $E_{vib}^{\mathrm{Ti_{54}H}}(T)$ is the vibrational energy of $Ti_{54}H$ supercell, $E_{vib}^{\mathrm{Ti_{54}}}(T)$ is the vibrational energy of the corresponding Ti_{54} supercell with pure

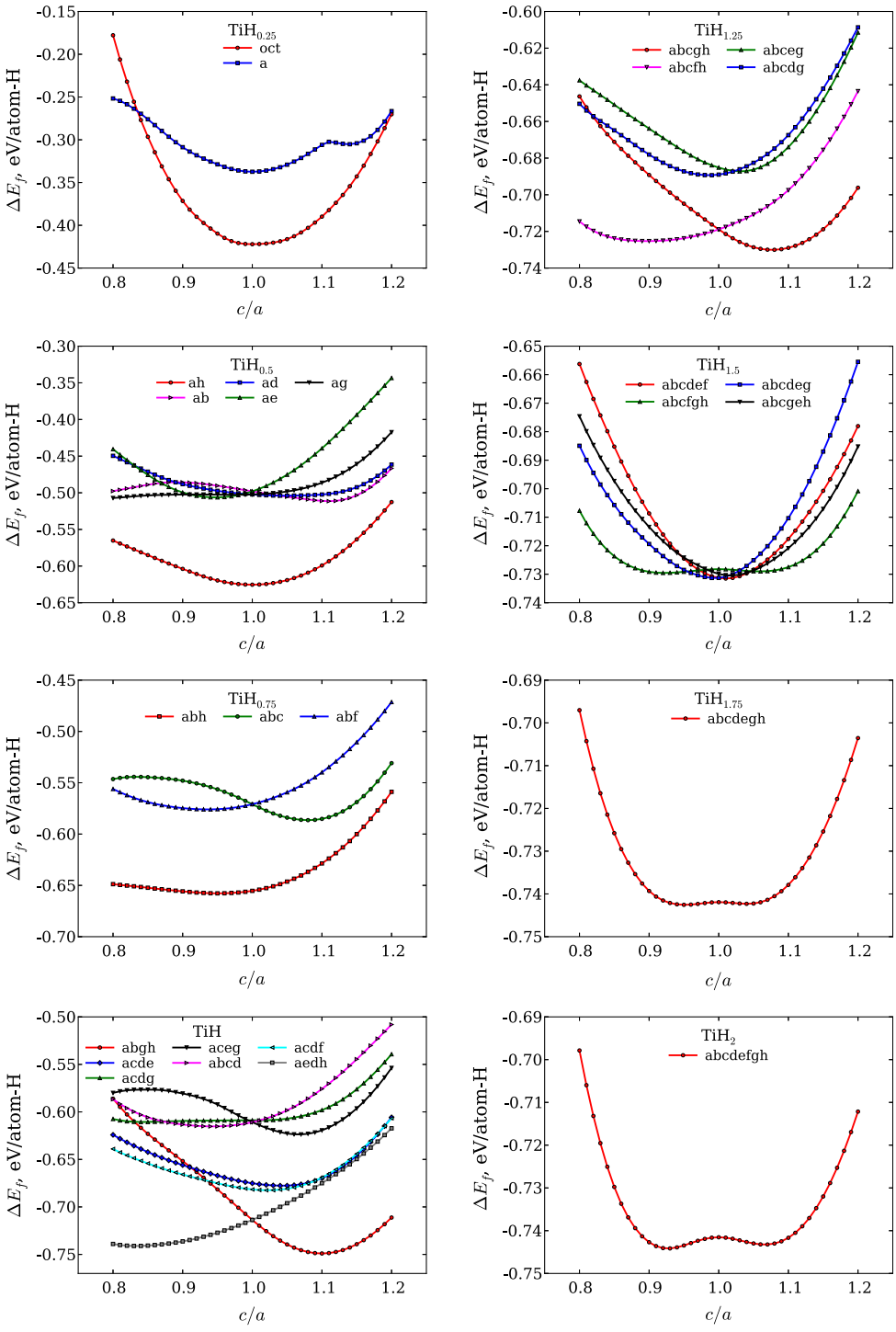

Fig. 2. Specific formation energies of TiH_x phases with non-equivalent arrangements of hydrogen atoms versus c/a ratio.

α-Ti, and $E^{H_2}(T)$ is the enthalpy of hydrogen gas at 0.1 MPa from the NIST database [35].

The dependence of the solution enthalpy $\Delta H_{sol}(T)$ on temperature in comparison to experimental data [3,60,61] (obtained from $P-C-T$ curves and Sievert's law) is shown in Fig. 4. It is evident that the solution enthalpy is almost constant throughout the entire range of temperatures, and DFT values are in harmony with the experiment. The experimental values of enthalpy differ from each other by up to 90 meV/atom-H (8.7 kJ/mol-H), and the predicted enthalpy lies in between those values. Since the temperature-dependent parts of hydrogen enthalpy in solid solution and molecule are compensating, it can be sufficient to calculate the solution enthalpy at 0 K. Small correction is provided by zero-point vibration energy (ZPE). According to our results, the $\Delta H_{sol}(T)$ is reduced by 45 meV/atom-H due to the ZPE of H in octahedral site of Ti, which is consistent with the calculated value (PAW GGA) of ~50 meV/atom-H by Aydin et al. [62].

While the solution enthalpy is almost independent of temperature, the dependence of solution free energy on T should be much more pronounced due to the vibrational entropy contribution. We define the standard free energy of solution of hydrogen in hcp lattice of titanium as

Table 2
Formation energies ΔH_f (kJ/mol-Ti) and lattice constants (Å) of titanium hydrides obtained with ABINIT code in comparison with *ab initio* and experimental results. In ABINIT, for hydrogen molecule we obtained –31.733 eV for the full energy in vacuum, 4.532 eV for cohesive energy, and 0.751 Å for H–H bond length.

Phase	Method	a	c/a	ΔH_f
γ-TiH	GGA (our)	4.172	1.10	−72.3
γ-TiH	GGA ([42])	4.164	1.10	−81.8
γ-TiH	GGA ([36])	–	1.10	−77.5
γ-TiH	GGA ([14])	4.168	1.10	–
γ-TiH	Exp. ([5])	4.210	1.09	–
γ-TiH	Exp. ([55])	4.199	1.09	–
γ-TiH	Exp. ([56])	4.190	1.12	–
γ-$TiH_{1.25}$	GGA (our)	4.228	1.08	−88.1
γ-$TiH_{1.25}$	GGA ([42])	4.226	1.08	−99.4
γ-$TiH_{1.25}$	GGA ([36])	–	1.08	−93.9
γ-$TiH_{1.5}$	GGA (our)	4.354	1.01	−105.9
γ-$TiH_{1.5}$	GGA ([42])	4.360	1.01	−118.8
δ-$TiH_{1.5}$	GGA (our)	4.369	1.00	−105.8
δ-$TiH_{1.5}$	GGA ([36])	–	1.00	−111.7
ϵ-$TiH_{1.5}$	GGA (our)	4.420	0.99	−105.8
ϵ-$TiH_{1.5}$	Exp. ([47])	4.406	0.97	–
ϵ-$TiH_{1.75}$	GGA (our)	4.471	0.95	−125.4
ϵ-$TiH_{1.75}$	GGA ([42])	4.467	0.95	−140.2
ϵ-$TiH_{1.75}$	Exp. ([57])	4.471	0.98	–
δ-$TiH_{1.75}$	GGA (our)	4.397	1.00	−125.3
δ-$TiH_{1.75}$	GGA ([36])	–	1.00	−131.5
δ-$TiH_{1.75}$	Exp. ([58])	4.425	1.00	–
ϵ-TiH_2	GGA (our)	4.524	0.93	−143.6
ϵ-TiH_2	GGA ([42])	4.517	0.93	−160.3
ϵ-TiH_2	Exp. ([45])	4.528	0.95	–
ϵ-TiH_2	Exp. ([46])	4.490	0.97	–
ϵ-TiH_2	Exp. ([41])	4.483	0.97	–
ϵ-TiH_2	Exp. ([47])	4.485	0.97	–
δ-TiH_2	GGA (our)	4.420	1.00	−143.1
δ-TiH_2	GGA ([36])	4.400	1.00	−149.5
δ-TiH_2	GGA ([42])	4.437	1.00	−160.2
δ-TiH_2	GGA ([14])	4.414	1.00	–
δ-TiH_2	Exp. ([45])	4.454	1.00	–
δ-TiH_2	Exp. ([55])	4.440	1.00	–

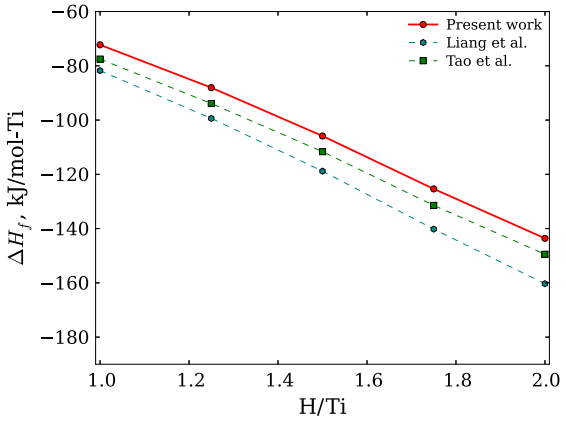

Fig. 3. Formation energies of Ti-H phases per one Ti atom in comparison with DFT results of Liang et al. [42] and Tao et al. [36].

$$\Delta F_{sol}(T) = \Delta E_{sol} + F_{vib}^{Ti_{54}H}(T) - F_{vib}^{Ti_{54}}(T) - \frac{1}{2}F^{H_2}(T), \quad (7)$$

where $F_{vib}^{Ti_{54}H}(T)$ is the vibrational free energy of $Ti_{54}H$ supercell, $F_{vib}^{Ti_{54}}(T)$ is the vibrational free energy of the corresponding supercell with pure hcp titanium and $F^{H_2}(T)$ is the free energy of hydrogen molecule taken from NIST database [35]. The temperature dependence of the standard free energy (ΔF_{sol}) is shown in Fig. 5. It is evident that the ΔF_{sol} quickly increases with temperature due to the higher entropy of hydrogen in H_2 molecule than in solid solution. For comparison, we provided, in Fig. 5, the standard free energy of H solution in zirconium, calculated with PAW GGA by Christensen et al. [63].

Table 3
Formation $E_f^{vac,n}$ and trapping ΔE^{trap} energies of vacancy and H-vacancy complexes in hcp titanium with respect to pure titanium and hydrogen in octahedral site. The number of configurations (N_{conf}) used for calculation of configuration entropy is also given.

System	N_{conf}	ΔE^{trap}	$E_f^{vac,n}$	$E_f^{vac,n}$ [19]
Empty	1	–	2.12	1.96
1 H	6	−0.26	1.86	1.73
2 H	15	−0.25	1.61	1.44
3 H	20	−0.38	1.23	1.16
4 H	15	−0.08	1.15	–
5 H	6	0.05	1.20	1.19

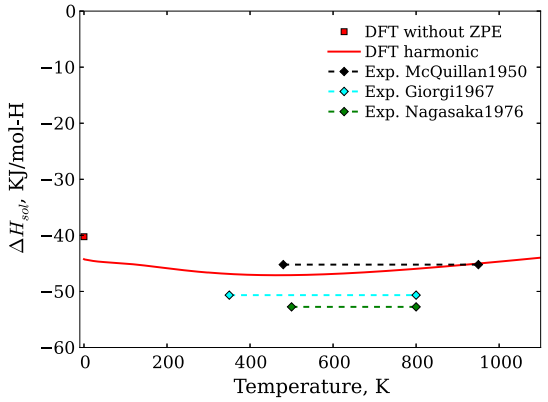

Fig. 4. Solution enthalpy of hydrogen in octahedral site of α-Ti relative to H_2 gas at 0 K and finite temperatures in comparison to experimental data [3,60,61].

4.2. Free energy of titanium hydrides

The temperature dependencies of the vibrational enthalpy ($E_{vib}(T)$) and entropy ($S_{vib}(T)$) of the three titanium hydrides TiH, $TiH_{1.5}$ and TiH_2 as compared to experiment and first-principles quasiharmonic results are shown in Figs. 6 and 7.

The agreement between our results and experimental data for TiH_2 hydride is quite good. At 600 K the differences between calculated and experimental values are ∼1.5 kJ/mole-Ti and ∼4 J/K/mole-Ti for enthalpy and entropy, respectively. The increased with temperature discrepancies are due to the anharmonicity and electron contributions. For example, the enthalpy and entropy of Ti hydrides obtained by Olsson et al. [59] are closer to the experimental values due to the temperature-dependent electron contributions.

It is evident from Figs. 6 and 7 that enthalpy and entropy for δ-TiH_2 are very close to enthalpy and entropy of ϵ-TiH_2.

Finally, we estimate the influence of vibrational energy on the formation enthalpies of titanium hydrides according to the following expression

$$\Delta H_f(T) = \Delta H_f + [E_{vib}^{Ti_{32}H_{32x}}(T) - E_{vib}^{Ti_{32}}(T)]/32 - xE_{vib}^{H_2}(T)/2.$$

The dependence of $\Delta H_f(T)$ on temperature is shown in comparison to the available experimental data in Fig. 8.

It can be seen from Fig. 8 that formation enthalpy of titanium hydrides slightly decreases until the temperature of 600 K in agreement with experiment. At higher temperatures, $\Delta H_f(T)$ is almost constant. The zero-point vibrational energy increases the formation enthalpy of δ-TiH_2 hydride by ∼90 meV/atom-H, making it more stable than γ-TiH hydride, the formation enthalpy of which is increased by ∼100 meV/atom-H. The effect of δ-TiH_2 stabilization in relation to γ-TiH due to the ZPE is in agreement with recent PAW GGA calculations [14,64].

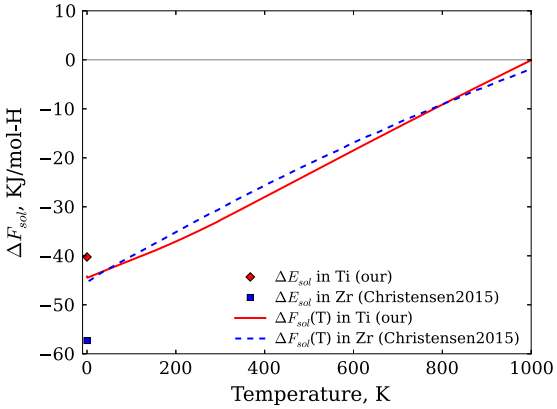

Fig. 5. Standard free energy of solution of hydrogen in octahedral sites of hcp-Ti lattice relative to H_2 molecule at 0 K and finite temperatures in comparison with that for hcp-Zr [63].

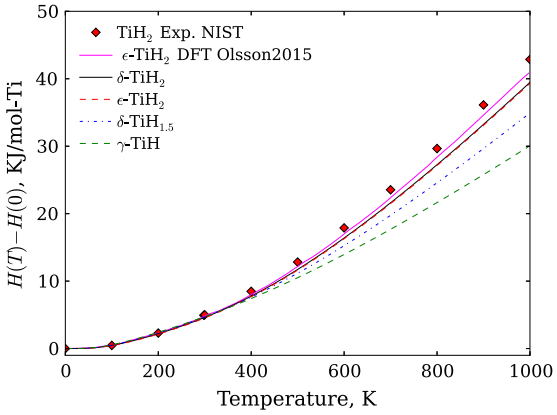

Fig. 6. Vibrational enthalpy of TiH, $TiH_{1.5}$ and TiH_2 hydrides calculated within harmonic approximation in comparison to experimental data from NIST database [35] and DFT results [59]. At zero pressure $H(T)$ is equal to $E(T)$.

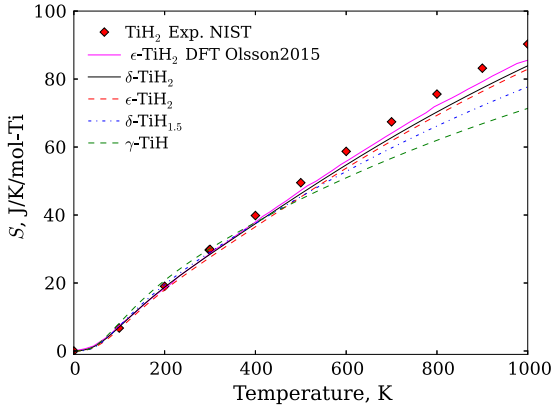

Fig. 7. Vibrational entropy of TiH, $TiH_{1.5}$ and TiH_2 hydrides calculated within harmonic approximation in comparison to experimental data from NIST database [35] and DFT results [59].

4.3. Discussion of δ-TiH_2 hydride instability and its influence on thermal properties

Several points should be noted about the thermodynamic properties of δ-TiH_2. It is known that this hydride is mechanically unstable at 0 K [14], which also can be seen from Fig. 2 (TiH_2 with $c/a = 1$ is characterised with local energy maximum). Normally, if a phase has some instability, its phonon dispersion curves would contain imaginary modes near the Gamma point. However, in the current study for δ-TiH_2 no imaginary modes were observed. This is in agreement with Xu et al. [14], where the same relatively small $2 \times 2 \times 2$ cubic supercell (32 Ti atoms) for δ-TiH_2 hydride was used, and no imaginary modes were revealed.

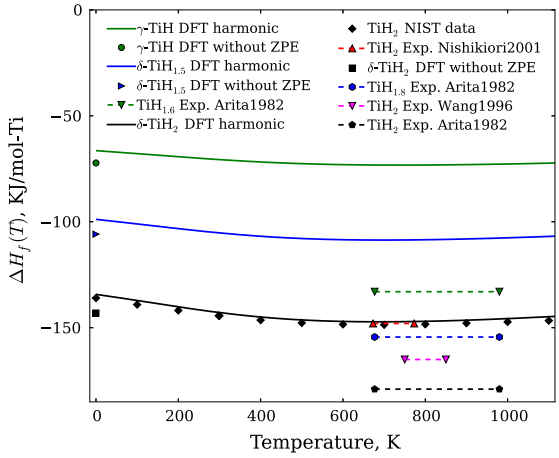

Fig. 8. Formation enthalpy of TiH, $TiH_{1.5}$ and TiH_2 hydrides in comparison to experimental data from NIST database [35] and several experimental works [15,65,66].

To understand the reasons of such behavior, we made additional calculations of the phonon dispersion curves and corresponding vibrational free energies using a larger $3 \times 3 \times 3$ cubic supercell (108 Ti atoms) for δ-TiH_2 phase and stable tetragonal ϵ-TiH_2 phase. First of all, we found that for stable ϵ-TiH_2 phase, the difference between the free energies for $3 \times 3 \times 3$ and $2 \times 2 \times 2$ supercells is less than 1 meV/atom-H in the studied temperature range. This confirms that for our purposes, it is adequate to use $2 \times 2 \times 2$ supercell. Secondly, noticeable imaginary modes appeared near the Gamma point in the case of unstable cubic δ-TiH_2 $3 \times 3 \times 3$ supercell. The existence of imaginary modes for larger supercell confirms the assumption made by Xu et al. [14] that if the force constants are too short ranged, the harmonic spring model fails to predict instabilities.

Moreover, we found that the reduction of smearing width from 0.2 to 0.008 eV reveals a few imaginary modes even in the case of $2 \times 2 \times 2$ supercell. This is in agreement with the density functional perturbation theory results of Ivashchenko et al., according to which imaginary modes on phonon dispersion curve of δ-TiH_2 disappear with the increase of smearing width [67]. It is known that instability of cubic δ-TiH_2 hydride is associated to the splitting of two degenerate electronic bands near the Fermi level, known as Jahn–Teller effect. With the increase in temperature, the Jahn–Teller effect becomes less expressed until it completely vanishes due to the smearing of the Fermi level. It is important that the reduction of smearing width has only negligible influence (1 meV/atom-H) on the vibrational free energy of δ-TiH_2 phase (omitting imaginary modes during the calculation of the free energy).

In the framework of the adopted approaches, we could not quantitatively estimate the error made in the calculation of free energy due to the exclusion of long-wavelength vibrations, which are partly responsible for δ-TiH_2 instability. However, small degree of instability (the difference of total energies at 0 K between δ-TiH_2 and ϵ-TiH_2 is less than 3 meV/atom-H), good agreement of calculated and experimental thermodynamic properties, and success in predicting hydrogen solubility allows us to claim that short-ranged harmonic spring model in the case of δ-TiH_2 is reliable enough for our objectives.

5. Solubility of hydrogen in α-titanium

It is known from the experiment [8] that at 600 K the solubility of hydrogen in α-Ti is ~6.7 at.%. However, in the recent thermodynamic assessment based on zero Kelvin first-principles results, the obtained solubility of H was of the order of 1 at.% [14].

The reasons for the disagreement between the experiment and theory could be owing to the superabundant vacancies filled with hydrogen and the influence of H vibrational free energy. Hence, with further steps, we successively estimated the impact of both effects on the H solubility. By doing so we: (i) utilized approximation of dilute solution; (ii) took into account that hydrogen could be both in octahedral and tetrahedral sites; (iii) assumed that in the entire range of temperatures, the solution of H in octahedral site is by 64 meV/atom more favorable than in the tetrahedral site of α-Ti.

5.1. The influence of H-vacancy complexes on the solubility of hydrogen

In Section 3.4, the formation energies of H-vacancy complexes in α-Ti at 0 K are provided. It follows that up to four H atoms can be trapped in the vacancy with the reduction of total energy. Such behavior could lead to the increase in hydrogen solubility and the formation of superabundant vacancies.

To check the influence of SAV effect on the solubility of hydrogen and concentration of vacancies, we used recently developed thermodynamic model based on grand canonical ensemble [23]. Since the solubility of hydrogen in Ti-H system is defined by the equilibrium between hydride and H solid solution, it is more convenient for us to use imaginable TiH_x hydride phase as a reservoir of hydrogen. For this reservoir, we define the formation energy of hydride per one H atom as

$$\Delta\mu_0 = \mu(H_{hydride,0}) - \mu(H_{sol,0}),$$

where μ contributions are defined through the total energies of the corresponding structures related to hydrogen molecule:

$$\mu(H_{hydride,0}) = \Delta E_f = [E(TiH_2) - E(Ti)]/2 - E(H_2)/2,$$

and

$$\mu(H_{sol,0}) = \Delta E_{sol} = [E(Ti_{54}H) - E(Ti_{54})] - E(H_2)/2.$$

Here we assume that $\Delta\mu_0$ is independent of temperature and could be calculated for 0 K. The minimization of grand canonical potential for this Ti-H system allows to calculate the vacancy concentrations (see Eq. (21) in [23]), which are shown in Fig. 9 depending on $\Delta\mu_0$ for 600 K.

It could be seen from Fig. 9 that in the region of realistic TiH_x formation energies ($\Delta\mu_0$), the main contribution to the vacancy concentration is due to the complexes with three H atoms. The concentrations of empty vacancies and vacancies with one, two, and four H atoms are lower by several orders. At 600 K and $\Delta\mu_0 = -0.2$ eV/atom-H, the concentration of H-vacancy complexes due the SAV effect is higher than that of empty vacancies by four orders. Obviously, this significant increase in vacancy concentration would have a pronounced effect on the diffusion controlled characteristics of Ti-H alloys.

The temperature dependencies of vacancy concentrations for fixed $\Delta\mu_0 = -0.2$ eV/atom-H (see Fig. 10) indicate that at lower temperatures, the increase in vacancy concentration is even more pronounced reaching seven orders at 300 K.

Finally, we estimated the influence of SAV effect on the solubility of hydrogen in α-Ti relative to δ-TiH_2 hydride with $\Delta\mu_0 = -0.317$ eV/atom-H. The hydrogen concentration (y_H) can be written as

$$y_H = \frac{A}{1 + \exp\left(-\frac{\Delta\mu}{k_B T}\right)}, \quad (8)$$

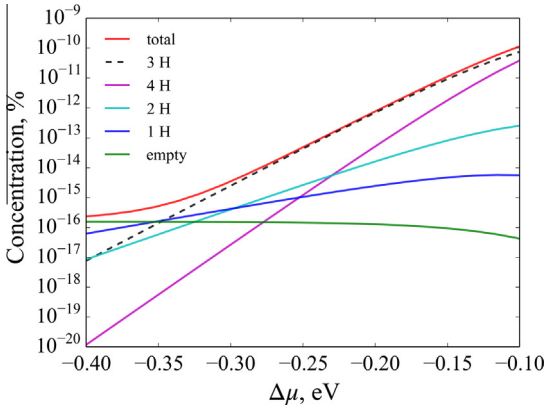

Fig. 9. Concentration of H-vacancy complexes depending on the formation energy of imaginable TiH_x hydride at 600 K. The complexes include pure vacancies and vacancies with 1–4 H atoms.

where A is the parameter, which takes into account vacancy concentration and configurational corrections as defined in [23]. In general, $\Delta\mu$ depends upon temperature, but here we put it equal to $\Delta\mu_0$.

The visualization of y_H in dependence of temperature (see Fig. 11) with and without hydrogen in vacancies shows no difference in the considered temperature range. The obtained terminal solubility at 600 K (0.34 at.%) is in agreement with Xu et al. [14] as well as much lower than the experimental value at that temperature. From this, we conclude that despite the pronounced influence of SAV effect on the concentration of vacancies, it could not be responsible for the higher solubility of hydrogen.

5.2. The influence of vibrational energy on the solubility of hydrogen in α-Ti

To estimate the influence of vibrational free energy on solubility, we calculated the dependence of

$$\Delta\mu = \Delta\mu_0 + \Delta\mu_{vib}$$

on temperature and substituted it into the Eq. (8). It is convenient to separate the $\Delta\mu$ into vibrational free energy of hydrogen in solution

$$\mu(H_{sol,vib}) = F_{vib}(Ti_{54}H) - F_{vib}(Ti_{54}) + \mu(H_{sol,0}),$$

and vibrational free energy of hydrogen in hydride

$$\mu(H_{hydride,vib}) = [F_{vib}(TiH_2) - F_{vib}(Ti)]/2 + \mu(H_{hydride,0}).$$

The calculated temperature dependencies of $\mu(H_{sol,vib})$ and $\mu(H_{hydride,vib})$ are shown in Fig. 12, from which the values of $\Delta\mu$ at each temperature could be calculated as $\mu(H_{hydride,vib}) - \mu(H_{sol,vib})$.

It is evident from Fig. 12 that the $\Delta\mu$ becomes smaller with temperature due to the larger slope of $\mu(H_{sol,vib})$. This is associated to the higher values of hydrogen vibrational entropy in solution.

The terminal solubility calculated with the account of vibrational energy in comparison to experimental data is shown in Fig. 13. The solubility, now, is much larger than in the case of fixed $\Delta\mu$ obtained for zero temperature and two times larger than the experimental value at 600 K. It is, however, known that δ-hydride is highly non-stoichiometric phase, and there is additional contribution of configurational entropy due to the vacancies in hydride. To make qualitative estimation of this influence, we added $k_B T ln(0.5)$ to the $\Delta\mu$. The resulted solubility curve is also shown in Fig. 13 and it better agrees with experiment.

We can conclude that the vibrational free energy has significant effect on the solubility limit of hydrogen in α-Ti. However, for more precise predictions of terminal solubility, several issues should be addressed more carefully. For example, in addition to configurational entropy of hydrides, the solubility quite noticeably depends

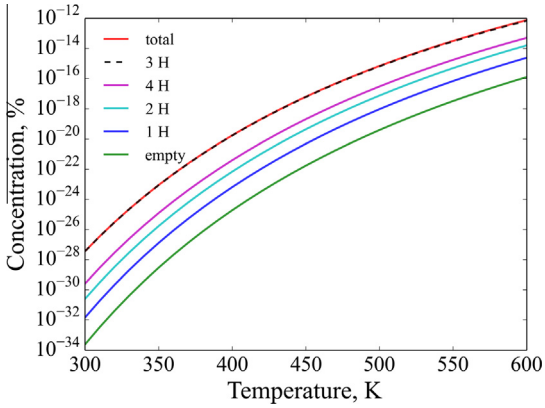

Fig. 10. Temperature dependence of H-vacancy complexes concentrations for $\Delta\mu_0 = -0.2$ eV/atom-H. The complexes include pure vacancies and vacancies with 1–4 H atoms.

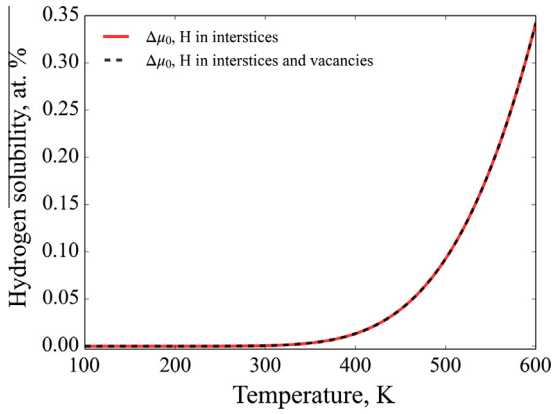

Fig. 11. The solubility of hydrogen in α-Ti. The amount of hydrogen in H-vacancy complexes is negligible in comparison to the amount of hydrogen in interstitials, and does not change the solubility curve.

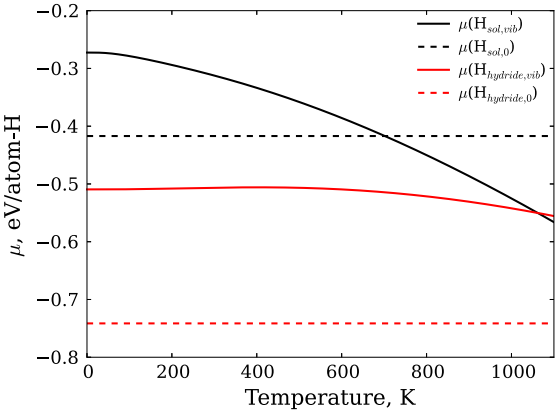

Fig. 12. Temperature dependence of solution free energy of hydrogen and formation free energy of titanium hydride δ-TiH_2 per one H atom. The dashed lines indicate the values of energies obtained for 0 K without zero-point vibrations. The difference $\mu(H_{hydride,vib}) - \mu(H_{sol,vib})$ is equal to the formation free energy of hydride with respect to hydrogen in octahedral site of hcp Ti.

on the difference between solution energies of hydrogen in octahedral and tetrahedral voids ($\Delta H_{oct/tet}$), and it is important to check the dependence of $\Delta H_{oct/tet}$ on temperature. For example, in Zr, moderate dependence of $\Delta H_{oct/tet}$ was found [63].

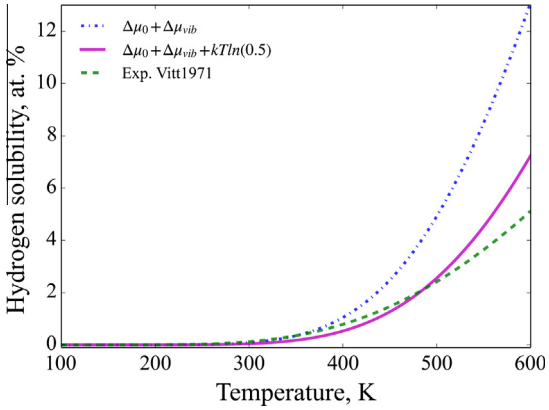

Fig. 13. The solubility of hydrogen in α-Ti with the account of vibrational free energy of solid solution and δ-TiH_2. To estimate the influence of TiH_x configurational entropy on the H solubility, the $k_BTln(0.5)$ term is added to the chemical potential of titanium hydride. The experimental data is taken from [4].

Finally, the approximation of dilute solution can also be the source of errors. For example, at concentrations as high as 7 at.%, the interaction between H atoms can increase the vibrational free energy resulting in moderate reduction of H solubility. On the other hand, the ordering of solid solution accompanied with the additional gain in solution enthalpy could lead to the higher hydrogen concentrations.

6. Conclusions

We revised the Ti-H system at finite temperatures using the combination of harmonic approximation and density functional theory (PAW GGA). To predict the solubility of hydrogen in α-Ti and its impact on the concentration of vacancies, we considered hydrogen solid solution in α-Ti at finite temperatures, H-vacancy complexes in α-Ti at 0 K, and experimentally known titanium hydrides at finite temperatures.

The solution of hydrogen was considered both in octahedral and tetrahedral sites at 0 K. The calculated value of hydrogen solution enthalpy in octahedral sites relative to H_2 molecule (-0.425 eV for $Ti_{96}H$) agrees well with the experiment and by 64 meV is lower than that in tetrahedral sites. While the solution enthalpy is almost constant, the vibrational free energy of H atom in α-Ti quite noticeably reduces with temperature.

To study the influence of H on vacancy concentrations, we considered several H-vacancy complexes. The calculated formation energy of pure vacancy at 0 K is 2.12 eV. We found that up to four hydrogen atoms could go from the octahedral site to the vacancy with the reduction of total energy. The trapping energies for the first, second, third and fourth added H atom in Ti vacancy are $-0.26, -0.25, -0.38$, and -0.08 eV, respectively. As a result, the effective formation energy of vacancy complex with 4 H atoms is 1.15 eV.

To find the most favorable titanium hydride for precipitation in α-Ti, we considered 27 titanium hydrides and investigated the dependence of formation energy on c/a ratio of lattice constants. It was found that, depending on stoichiometry, it could be one or two close minima observed for $c/a < 1$ and $c/a > 1$. The most favorable hydride at 0 K, if the formation energy is calculated per one H atom relative to H solid solution ($Ti_{54}H$), is γ-TiH. Its formation energy is -0.325 eV/atom-H, while the energy of δ-TiH_2 and ϵ-TiH_2 are by 8 meV and 5 meV higher, respectively. However, with the account of zero-point vibration energies, γ-TiH becomes less favorable than δ-TiH_2 (-0.223 eV/atom-H and -0.230 eV/atom-H, respectively).

Finally, to estimate the temperature dependence of hydrogen solubility relative to δ-TiH_2 hydride and the concentration of vacancies, we have used a thermodynamic model, which was developed for the description of superabundant vacancy formation [23]. According to our results, the concentration of complexes with three H atoms is much higher than that of other H-vacancy configurations. For example, at 600 K and hydride formation energy of −0.2 eV/atom-H, the vacancy concentration increases by four orders, which should have a prominent effect on diffusion properties, but does not have an influence on the H solubility.

On the other hand, we have discovered that the account of vibrational contributions to the free energy increases the solubility of hydrogen by more than one order. For example, after the vibrational energy had been taken into account, the predicted value of H solubility at 600 K (7.2 at.%) became very close to that obtained in experiments (∼6.7 at.% [7] and ∼5.1 at.% [4]).

Acknowledgment

The authors gratefully acknowledge support from the Ministry of Education and Science of the Russian Federation through the Contract No. 3.1282.2014K.

References

[1] E. Tal-Gutelmacher, D. Eliezer, JOM 57 (2005) 46–49.
[2] F.H. Froes, O.N. Senkov, J.I. Qazi, Int. Mater. Rev. 49 (2004) 227–245.
[3] A.D. McQuillan, Proc. R. Soc. A Math. Phys. Eng. Sci. 204 (1950) 309–323.
[4] R.S. Vitt, K. Ono, Metall. Trans. 2 (1971) 608–609.
[5] H. Numakura, M. Koiwa, Acta Metall. 32 (1984) 1799–1807.
[6] D.S. Shih, I.M. Robertson, H.K. Birnbaum, Acta Metall. 36 (1988) 111–124.
[7] D. Setoyama, J. Matsunaga, H. Muta, M. Uno, S. Yamanaka, J. Alloys Compd. 381 (2004) 215–220.
[8] D. Setoyama, J. Matsunaga, H. Muta, M. Uno, S. Yamanaka, J. Alloys Compd. 385 (2004) 156–159.
[9] M.I. Luppo, A. Politi, G. Vigna, Acta Mater. 53 (2005) 4987–4996.
[10] Y. Fukai, J. Alloys Compd. 404–406 (2005) 7–15.
[11] Y.R. Kolobov, V.I. Torganchuk, V.N. Fokin, B.P. Tarasov, IOP Conf. Ser. Mater. Sci. Eng. 81 (2015) 012053.
[12] G.A. Young, J.R. Scully, Scr. Metall. Mater. 28 (1993) 507–512.
[13] J.E. Costa, J.C. Williams, a.W. Thompson, Metall. Trans. A 18 (1987) 1421–1430.
[14] Q. Xu, A. Van der Ven, Phys. Rev. B 76 (2007) 064207.
[15] W.-E. Wang, J. Alloys Compd. 238 (1996) 6–12.
[16] S. Ukita, H. Ohtani, M. Hasebe, J. Jpn. Inst. Met. 71 (2007) 721–729.
[17] E. Königsberger, G. Eriksson, W.A. Oates, J. Alloys Compd. 299 (2000) 148–152.
[18] K. Wang, X. Kong, J. Du, C. Li, Z. Li, Z. Wu, Calphad 34 (2010) 317–323.
[19] D. Connétable, J. Huez, E. Andrieu, C. Mijoule, J. Phys. Condens. Matter 23 (2011) 405401.
[20] A.Y. Kuksin, A.S. Rokhmanenkov, V.V. Stegailov, Phys. Solid State 55 (2013) 367–372.
[21] X. Han, Q. Wang, D. Sun, H. Zhang, Scr. Mater. 56 (2007) 77–80.
[22] K. Nakamura, Y. Fukai, J. Alloys Compd. 231 (1995) 46–50.
[23] R. Nazarov, T. Hickel, J. Neugebauer, Phys. Rev. B 82 (2010) 224104.
[24] X. Gonze, J.M. Beuken, R. Caracas, F. Detraux, M. Fuchs, G.M. Rignanese, L. Sindic, M. Verstraete, G. Zerah, F. Jollet, M. Torrent, A. Roy, M. Mikami, P. Ghosez, J.-Y. Raty, D. Allan, Comput. Mater. Sci. 25 (2002) 478–492.
[25] G. Kresse, J. Furthmüller, Comput. Mater. Sci. 6 (1996) 15–50.
[26] P. Hohenberg, Phys. Rev. 136 (1964) B864–B871.
[27] W. Kohn, L.J. Sham, Phys. Rev. 140 (1965) A1133–A1138.
[28] P.E. Blöchl, Phys. Rev. B 50 (1994) 17953–17979.
[29] J.P. Perdew, K. Burke, M. Ernzerhof, Phys. Rev. Lett. 77 (1996) 3865–3868.
[30] M. Methfessel, A.T. Paxton, Phys. Rev. B 40 (1989) 3616–3621.
[31] L. Verlet, Phys. Rev. 159 (1967) 98–103.
[32] D.J. Evans, B.L. Holian, J. Chem. Phys. 83 (1985) 4069.
[33] J.D. Head, M.C. Zerner, Chem. Phys. Lett. 122 (1985) 264–270.
[34] A. Togo, F. Oba, I. Tanaka, Phys. Rev. B 78 (2008) 134106.
[35] M. Chase, J. Phys. Chem. Ref. Data Monograph (1998).
[36] S. Tao, P. Notten, R. van Santen, A. Jansen, Phys. Rev. B 79 (2009) 144121.
[37] R.R. Pawar, V.T. Deshpande, Acta Crystallogr. Sec. A 24 (1968) 316–317.
[38] D.A. Aksyonov, A.G. Lipnitskii, Y.R. Kolobov, Model. Simul. Mater. Sci. Eng. 21 (2013) 075009.
[39] R. Matsumoto, M. Sera, N. Miyazaki, Comput. Mater. Sci. 91 (2014) 211–222.
[40] B. Baranowski, S. Majchrzak, T.B. Flanagan, J. Phys. F: Met. Phys. 1 (1971) 258–261.
[41] P.E. Irving, C.J. Beevers, Metall. Trans. 2 (1971) 613–615.
[42] C.P. Liang, H.R. Gong, J. Appl. Phys. 114 (2013) 43510.
[43] A. San-Martin, F.D. Manchester, Bull. Alloy Phase Diagrams 8 (1987) 30–42.
[44] H. Okamoto, J. Phase Equilibria Diffus. 32 (2011) 174–175.
[45] H.L. Yakel, Acta Crystallogr. 11 (1958) 46–51.
[46] R.L. Crane, S.C. Chattoraj, M.B. Strope, J. Less Common Met. 25 (1971) 225–227.
[47] C. Korn, Phys. Rev. B 28 (1983) 95–111.
[48] O.T. Woo, G.C. Weatherly, C.E. Coleman, R.W. Gilbert, Acta Metall. 33 (1985) 1897–1906.
[49] A. Bourret, A. Lasalmonie, S. Naka, Scr. Metall. 20 (1986) 861–866.
[50] H. Numakura, M. Koiwa, H. Asano, H. Murata, F. Izumi, Scr. Metall. 20 (1986) 213–216.
[51] C. Zhang, Q. Kang, Z. Lai, R. Ji, Acta Mater. 44 (1996) 1077–1084.
[52] R. Ding, I.P. Jones, J. Electron Microsc. (Tokyo) 60 (2011) 1–9.
[53] Z. Li, P. Ou, N. Sun, Z. Li, A. Shan, Mater. Lett. 105 (2013) 16–19.
[54] C.P. Liang, H.R. Gong, Mater. Lett. 115 (2014) 252–255.
[55] T. Wang, F. Eichhorn, D. Grambole, R. Grotzschel, F. Herrmann, U. Kreissig, W. Moller, J. Phys. Condens. Matter 14 (2002) 11605–11614.
[56] S.R. Peddada, I.M. Robertson, H.K. Birnbaum, J. Mater. Res. 8 (1993) 291–296.
[57] H. Zhang, E.H. Kisi, J. Phys. Condens. Matter 9 (1997) L185–L190.
[58] P. Millenbach, M. Givon, J. Less Common Met. 87 (1982) 179–184.
[59] P.A.T. Olsson, J. Blomqvist, C. Bjerkén, A.R. Massih, Comput. Mater. Sci. 97 (2015) 263–275.
[60] M. Nagasaka, T. Yamashina, J. Less Common Met. 45 (1976) 53–62.
[61] T.A. Giorgi, F. Ricca, Nuovo Cim. 5 (Suppl. (1)) (1967) 472–482.
[62] U. Aydin, L. Ismer, T. Hickel, J. Neugebauer, Phys. Rev. B 85 (2012) 155144.
[63] M. Christensen, W. Wolf, C. Freeman, E. Wimmer, R.B. Adamson, L. Hallstadius, P.E. Cantonwine, E.V. Mader, J. Phys. Condens. Matter 27 (2015) 25402.
[64] C.H. Hu, D.M. Chen, Y.M. Wang, K. Yang, , J. Alloys Compd. 450 (2008) 369–374.
[65] M. Arita, K. Shimizu, Y. Ichinose, Metall. Trans. A 13 (1982) 1329–1336.
[66] T. Nishikiori, T. Nohira, Y. Ito, J. Electrochem. Soc. 148 (2001) E38.
[67] V.I. Ivashchenko, L.A. Ivashchenko, P.L. Srynsckyy, L.A. Grishnova, A.I. Stegnyy, Ab initio study of the electronic structure and phonon dispersions For TiH_2 and ZrH_2, in: B. Baranowski, S.Y. Zaginaichenko, D.V. Schur, V.V. Skorokhod, A. Veziroglu (Eds.), Carbon Nanomater. Clean Energy Hydrog. Syst., NATO Science for Peace and Security Series C: Environmental Security, Springer, Netherlands, Dordrecht, 2009, pp. 705–712.